Research Square

Preprints are preliminary reports that have not undergone peer review.
They should not be considered conclusive, used to inform clinical practice,
or referenced by the media as validated information.

In silico investigation of valproic acid mediated GSK-3β inhibition and therapeutic mitigation of radiation induced intestinal injury

Prashasti Sharma
Homi Bhabha National Institute
Dharmendra Maurya
dkmaurya@barc.gov.in
Bhabha Atomic Research Centre

Research Article

Keywords: Glycogen synthase kinase-3β, Valproic acid, Wnt signaling, β-Catenin, Molecular docking, MD simulation

Posted Date: June 12th, 2026

DOI: https://doi.org/10.21203/rs.3.rs-10004634/v1

License: This work is licensed under a Creative Commons Attribution 4.0 International License.
Read Full License

Additional Declarations:
No competing interests reported.

Table 1 is available in the Supplementary Files section.

In silico investigation of valproic acid mediated GSK-3β inhibition and therapeutic mitigation of radiation induced intestinal injury

Prashasti Sharma[1, 2] and Dharmendra Kumar Maurya[1,2,]*

[1]Homi Bhabha National Institute, Anushaktinagar, Mumbai 400094, India

[2]Radiation Biology & Health Sciences Division, Bhabha Atomic Research Centre, Mumbai 400085, India

Corresponding author:

Dharmendra Kumar Maurya, Ph.D

Scientific Officer at Radiation Biology & Health Sciences Division, Bhabha Atomic Research Centre, Mumbai 400085, India

Associate professor at Homi Bhabha National Institute, Anushaktinagar Mumbai 400094, India. Email- dkmaurya@barc.gov.in

Abstract

Radiation-induced gastrointestinal injury is a dose-limiting complication of abdominal and pelvic radiotherapy, marked by epithelial loss, inflammation, and impaired regeneration. Glycogen synthase kinase-3β (GSK-3β), a negative regulator of canonical Wnt/β-catenin signaling, is central to intestinal stem cell maintenance and mucosal repair. Here, we evaluated valproic acid (VPA) as a modulator of GSK-3β using in silico docking and molecular dynamics, network biology, and in vivo irradiation models. Molecular docking analysis revealed favorable binding of VPA within the ATP-binding pocket of GSK-3β (binding free energy: -4.7 kcal/mol; estimated Ki: 0.36 mM). Notably, the predicted Ki falls within the clinically achievable therapeutic concentration range of VPA, supporting the potential for biologically relevant GSK-3β modulation in vivo. VPA interacted with residues implicated in ATP coordination, forming hydrogen bonds with Val139 and hydrophobic contacts with Gly67, Lys89, Asp137, and Tyr138. A 200-ns MD trajectory showed a stable VPA-GSK-3β complex and persistent hydrogen bonding, supporting electrostatic stabilization. MM/PBSA binding energies for VPA (-34.16 kcal/mol) was more favorable than the native ligand and known inhibitor (native: -33.9673 kcal/mol, known inhibitor: -31.273 kcal/mol). Principal component analysis revealed ligand-dependent shifts in conformational sampling, suggesting altered active-site dynamics rather than full blockade. PPI network analysis connected GSK-3β modulation to stabilization of β-catenin and attenuation of NF-κB-driven inflammation. In vivo, VPA (100 mg/kg.b.wt) increased survival after whole-body irradiation (66% vs. 33%) and preserved colon length following abdominal irradiation. Together, these results support a model in which VPA exerts moderate, indirect inhibition of GSK-3β that favors Wnt-mediated regeneration and reduces inflammatory responses in irradiated intestine.

Keywords: Glycogen synthase kinase-3β, Valproic acid, Wnt signaling, β-Catenin, Molecular docking, MD simulation

Introduction

Radiation therapy has a significant impact on the physiology and function of the gastrointestinal tract. Indeed, because of the high rate of renewal and rapid turnover of the epithelium, the small intestine is one of the most sensitive organs to accidental damage from irradiation [1, 2]. Damage to the small intestine is associated with disruption of barrier function, inflammation, depletion of progenitor cells in the crypts of Lieberkühn, loss of regenerative capacity, and ultimately the development of either acute enteritis or fibrosis of the mucosa. In spite of progress in radiotherapy techniques, which make it possible to increase its accuracy, there is still an urgent need for agents that can both stimulate the process of regeneration and reduce inflammation [3]. Research employing mouse and fruit fly models has significantly advanced knowledge of the role played by the Wnt signaling pathway in maintaining adult intestinal function and homeostasis [4]. The Wnt/β-catenin signaling pathway plays a crucial role in the control of self-renewal of epithelial stem cells, regulation of cellular differentiation, and maintenance of mucosal homeostasis [3, 5-7]. Wnt ligands stimulate their receptors, namely Frizzled receptors and LRP5/6 co-receptors. This leads to the suppression of the β-catenin destruction complex, which allows for its stabilization and translocation into the nucleus, followed by the stimulation of TCF/LEF-dependent transcriptional activity. Thus, Wnt stimulates the proliferation and repair of the epithelium. Importantly, glycogen synthase kinase-3β (GSK-3β), a serine/threonine kinase present in all cells, is an integral part of the destruction complex [8]. GSK3 exists as two closely related isoforms, GSK-3α and GSK-3β, both of which function as important inhibitory components of the Wnt/β-catenin signaling cascade [7]. Phosphorylation by GSK-3β determines the fate of β-catenin and is responsible for its degradation by the proteasome complex. Blockade of GSK-3β allows for β-catenin to be stabilized, translocated into the nucleus, and activates TCF/LEF-mediated transcription and, therefore, induces regenerative processes in the epithelium [9]. Moreover, GSK-3β takes part in inflammatory processes by interacting with NF-κB signaling pathways and regulating the expression of inflammatory cytokines [10]. An imbalance in GSK-3β signaling has been shown to be associated with enhanced intestinal inflammation, suggesting that inhibition of the kinase could lead to two beneficial outcomes, namely promotion of epithelial proliferation and down-regulation of inflammatory response. Preclinical studies showed that the use of small molecule inhibitors of GSK-3β (e.g., SB216763 and tideglusib) significantly reduced radiation enteropathy in preclinical models of gut inflammation [11].

Valproic acid (VPA) is a well-known anticonvulsant and mood stabilizer, which is often used for other purposes, including histone deacetylase inhibition, neuroprotection, and anti-inflammatory activity [12-14]. Importantly, VPA was found to inhibit GSK-3β and thus regulate the Wnt/β-catenin pathway. In a study, it was found that treatment of intestinal organoid with VPA treatment increased the number of LGR5+ stem cells and help in organoid regeneration after irradiation which suggest that the modulation of GSK-3β activity through treatment with VPA could have a beneficial effect on the survival and proliferation of intestinal stem cells [15]. The radioprotective effects of VPA was also observed in the rat brain protection were following X-ray irradiation [15, 16]. So VPA treatment might may be speed up epithelial cell restoration, and regulate inflammatory responses, thus serving as an adequate candidate for counteracting radiation-induced injury. However, the binding characteristics of VPA at the level of the atomic interface with GSK-3β and the overall effects of such binding in terms of systemic signaling cascades in the context of the radiation damage recovery process require clarification. In order to fill this gap, the current work utilized a combination of molecular docking and molecular dynamics (MD) simulations to analyze VPA's ability to bind to and interact with the active site of GSK-3β compared to known drugs. At the same time, PPI networks of the downstream effector molecules and their interactions were analyzed using STRING, which allowed us to outline the possible biological consequences of GSK-3β inactivation mediated by VPA. Further, preliminary in vivo study has been done to explore VPA's radioprotective effect by monitoring mice survival and restoration of the colon length.

Materials and Methods

Protein and ligand preparation: Human GSK-3β crystal structure (PDB ID: 1Q4L) was obtained from the PDB database (https://www.rcsb.org/). Crystallographic water molecules and all unnecessary heteroatoms were stripped off and missing residues were reconstructed based on the homology modelling using UCF Chimera [17]. Ligand (valproic acid, native ligand (679) of GSK-3β and its known inhibitor SB216763) structures were optimized for energy using the universal force field, and converted into PDBQT format.

Molecular docking: The molecular docking was performed using AutoDock Vina with the help of PyRx [18]. The binding box was defined using the coordinates of the native ligand binding site (x = 43.025, y = 13.282, z = 41.103, size = 38.837 × 41.013 × 50.955 Å). Exhaustiveness = 8 was applied to increase the thoroughness of the simulation. Best poses were ranked based on estimated

binding affinity (kcal/mol) and analyzed in Discovery Studio Visualizer in terms of potential 2D/3D interactions.

Molecular dynamics simulations: All-atom MD simulations were performed for GSK-3β with bound valproic acid, native ligand and the known inhibitor SB216763 using GROMACS 2019 [19]. The protein force fields were set according to CHARMM27, whereas the ligand parameter sets were obtained using the SwissParam server [20]. A solvation step added each complex to a cubic box with TIP3P water molecules and ensured a minimal distance of 12 Å from the protein's surface to the box's border. Then, the systems were neutralized and the ionic strength was set to physiological levels with sodium or chloride ions, depending on the system. Energy minimization continued until reaching the maximum force lower than 1000 kJ/mol/nm. Equilibration involved 100 ps of NVT equilibration at 310 K and an additional 100 ps of NPT equilibration at 310 K and 1 atm, utilizing the V-rescale thermostat and the Parrinello-Rahman barostat. Production simulations lasted 200 ns with a 2 fs timestep.

Analysis of simulation trajectories: Periodic artifacts were removed from the trajectories, which were then centered on the complex coordinates before analysis. Backbone and ligand stabilities were assessed using RMSD calculation (GROMACS rms). Protein and ligand per-residue flexibility was estimated using root-mean-square fluctuations (RMSF) in order to identify the regions of dynamics in the complex binding site. The compactness of the complex was measured using radius of gyration (gyrate). Radial distribution functions (rdf) were used to determine solvent and ion distribution close to the ligand and protein residue surfaces. Hydrogen bond formation between protein and ligand during the production run was analyzed with hbond (number, occupancy, and lifetime of interactions). The solvent accessible surface area (SASA) was computed (sasa) to measure conformational changes related to complex formation. The binding free energy for each complex was calculated using the Molecular Mechanics/Poisson-Boltzmann Surface Area (MM/PBSA) approach implemented in g_mmpbsa for representative and equilibrated frames [21]. Free energies of the interactions and energies of the van der Waals, electrostatic, polar, and non-polar components of solvation were decomposed per-residue-wise as well. Further individual amino acid total contributional energy in interaction of GSK-3β with it native ligand, known inhibitor SB216763 and VA was also calculated. By default, standard values of tool parameters were used, except when required to achieve sufficient statistical significance for each individual case.

Protein-protein interaction networks: Protein-protein interaction networks were constructed to evaluate VPA's putative protective mechanisms on intestinal epithelium. We assembled a seed list including validated VPA targets (histone deacetylases, (HDAC1/2), GABA transaminase (GABAT), GSK3β (GSK3B), β-catenin (CTNNB1), intestinal junctional proteins (CDH1, OCLN, CLDN1, TJP1/ZO-1) and injury/repair effectors (HIF1A, MYLK, VEGFA) [22-24]. Interaction data were retrieved from STRING v11.5 (https://string-db.org) using the "multiple proteins" input, species set to Homo sapiens, and a minimum interaction score of 0.7 (high confidence) [25, 26]. Compound–protein interaction data were retrieved from the STITCH 5.0 database ((http://stitch-db.org) using "valproate" as the query term, with the species set to Homo sapiens and a minimum interaction score of 0.7 (high confidence). The interaction tables obtained from both STRING and STITCH were imported into Cytoscape v3.10.3, and the networks were merged for subsequent analysis. Functional enrichment analyses of the VPA-associated seed proteins were performed using STRING v11.5. Gene Ontology (GO) categories, including Biological Process and Molecular Function, as well as Kyoto Encyclopedia of Genes and Genomes (KEGG) pathway annotations, were retrieved and analyzed.

Animals, irradiation, and VPA treatments: Swiss male mice (8-10-week-old; weight 25-28g) were housed under standard laboratory conditions. All experiments were approved by the BARC Animal Ethics Committee (BAEC/14/2024) Irradiations were performed with whole body irradiation (WBI) at a dose of 8.5 Gy by ^{60}Co-based Bhabhatron (dose rate, 1 Gy/min) as single fraction. For local abdominal irradiation, mice were exposed to 15 Gy to abdominal region with shielding to non-target sites. VPA was administered at the dosage of 100 mg/kg b. wt by oral gavage with the dosing protocol being single dose an hour after WBI irradiation followed by daily doses on 3 more consecutive days. Control mice were treated with vehicle only (n = 6 in each group). Mice were kept alive and observed for 30 days and their survival rates were calculated and compared by log-rank (Mantel-Cox) test. In abdominal irradiation experiment also VPA was administered at the dosage of 100 mg/kg b. wt by oral gavage as described above. Control mice were treated with vehicle only (n = 4 in each group). Mice were sacrificed anesthetically on 7th day after irradiation. Colons were removed, and cut out from cecum to rectum, measure it size and imaged. Data are shown as mean ± SEM and compared by t-test where $p < 0.05$ was regarded as significant.

Data visualization and statistics: All binding pose visualizations were generated using Discovery Studio Visualizer and all graphical figures such as RMSD, RMSF, gyrate, H-bonds, Radial diffusion and SASA plots were plotted on excel. Network diagrams were drawn using Cytoscape. Survival and colon length graph were plotted using GraphPad Prism 9, with $p < 0.05$ considered significant. Whenever applicable, data are shown as mean ± SEM, with sample size mentioned in the legends.

Results

Molecular docking of valproic acid, native ligand and known inhibitor to GSK-3β: The molecular docking of VPA revealed that VPA docked into the ATP binding site of GSK-3β having a free energy of binding with -4.7 kcal/mol, as compared to the native ligand and known inhibitor having a free energy of binding -8.5 and -7.5 kcal/mol, respectively. It binds within the overlapping region of the catalytic pocket where the native ligand is present (Fig 1). Binding of VPA occurs through residues involved in ATP binding. Predicted hydrogen bond interactions occur between VPA and Val135, whereas hydrophobic interactions occur between VPA and Gly67, Lys89, Asp137 and Tyr138, respectively.Notably, all amino acid residues involved in the interaction between VPA and GSK-3β were found to overlap with those engaged in the binding of GSK-3β to its native ligand and a well-characterized inhibitor. In contrast, however, the native ligand formed a more intricate network of interactions involving both hydrogen bonds, π-π stacking, and hydrophobic interactions (Fig 1). Hydrogen bonding between the ligand and receptor was found to be less extensive and the hydrophobic interactions to be relatively minor for VPA compared to the native ligand and known inhibitor, suggesting that it is less stable and may not completely block ATP. The results suggest that there is moderate inhibition at best.

Validation of the VPA-GSK-3β interaction through molecular dynamics: MD simulations on long time scales (200 ns) have shown that the VPA-GSK-3β complex adopts a stable configuration, demonstrating that there is significant binding between VPA and GSK-3β. As the simulation reached a steady-state after the equilibration process took place, backbone RMSD values stabilized at 0.20-0.30 nm. The RMSD value of the VPA was fairly constant from its location within the binding site, suggesting stable binding despite being not highly tight (Fig 2A). This was further verified by the RMSF value for residues at the ATP site which was much closed to native ligand and known inhibitors (Fig 2B). The radius of gyration did not change much during the course of the simulation (~2.22 - 2.24 nm), suggesting no significant unfolding and loosening of the

complex structure for VPA, native ligand and known inhibitor (Fig 2C). RDF calculations suggested the existence of structural water around the ligand, showing a g(r) value 4.117, 3.335 and 3.929 respectively for VPA, native ligand and known inhibitors respectively (Fig 2D). Hydrogen-bond analysis revealed persistent polar interactions that were maintained throughout a substantial portion of the simulation trajectory, contributing to the electrostatic stabilization of the protein-ligand complex. The average number of hydrogen bonds formed by VPA (H-bond No. 0.969) was higher to that observed for the known inhibitor (H-bond No. 0.636) but lower than that of the native ligand (H-bond No. 1.593) (Fig. 3A). Similarly, the solvent-accessible surface area (SASA) of the VPA-bound complex was 219.378 nm^2 which is comparable to that of the known inhibitor (219.536 nm^2), although it was higher than that of the native ligand bound complex (217.927 nm^2) (Fig. 3B).

Binding energy predictions through MM/PBSA method confirmed the docking results hierarchy, where the native ligand and know inhibitor provided a much more favorable ΔGbind than VPA (binding energies that correlate positively with a higher level of potency), while VPA exhibited binding energies with moderate favorability (less favorable but still biological significant). Binding energies through MM/PBSA calculations were -31.273, -33.967, and -34.16 kcal/mol for known inhibitor, native ligand and VPA respectively (Table 1). Contributions from binding energy components showed favorable contributions from van der Walls, Electrostatic energy, and SASA energy components along with an unfavorable solvation energy component due to polarity, and also pointed out some important residues which contributed disproportionately to binding energy. Binding energies through MM/PBSA calculations for VPA show better binding affinity to the GSK-3β ATP binding site compared with the native ligand and known inhibitor. This may be due to enough favorable interactions to stabilize the VPA to binding to the GSK-3β pocket. We further evaluated how individual GSK-3β residues contribute to the overall binding free energy of complexes formed with the native ligand, known inhibitors, and VPA (Fig 5). The results revealed that Ile66, Val74, Ala74, Leu136, Tyr138, Thr142, Arg148, Leu192, and Cys203 contribute substantially to ligand binding and play important roles in stabilizing the interactions between GSK-3β and the native ligand, known inhibitors, and VPA. In contrast, residues Val179, Glu141, Asp185, Lys187, Gln189, Asp194, and Asp204 exhibited positive energy contributions, suggesting they are less favorable for binding and may not participate directly in stabilizing ligand-protein interactions.

Analysis of the MD trajectories through PCA: The principal component analysis method was performed on the MD trajectories of the GSK-3β-ligand complexes to identify their significant collective dynamic properties. After the alignment of the MD trajectories, the covariance matrix for the positional fluctuations was computed based on the Cα- atom coordinates (Fig 4 A-C). The eigenvalues and eigenvectors obtained by eigenvalue decomposition of the covariance matrix (using gmx covar) describe the major modes of motion, which were then used in projection analysis (using gmx anaeig) to obtain visual representations of the conformations along the different modes of motion. The analysis was carried out using Cα- atom only, and normally, the first two or three modes explained most of the positional variance observed in these trajectories. PCA helps to identify correlated motions on a larger scale and define the conformational space visited during simulation, allowing for comparison of the dynamics fingerprints of the complexes in the presence and absence of the inhibitor.

Protein-protein interaction network implicates Wnt/β-catenin modulation: Although docking and MD indicate only moderate direct binding of VPA to the GSK-3β active site, published evidence for indirect regulation i.e most notably increased Ser9 phosphorylation of GSK-3β supports functional suppression of kinase activity and consequent stabilization of β-catenin in intestinal epithelia. This biochemical shift promotes Wnt pathway activation, enhances epithelial regeneration, and is associated with reduced NF-κB signaling and lower levels of pro-inflammatory cytokines (for example, TNF-α and IL-6), effects that have been reported in experimental models of intestinal injury and colitis. STRING/STRITCH-based PPI mapping centered on GSK-3β recovered canonical destruction-complex partners including CTNNB1 (β-catenin), AXIN1, and APC, along with downstream effectors linking Wnt signaling to cell proliferation and inflammatory regulation (Fig 5A). Functional enrichment analysis of the VPA-associated protein network revealed significant involvement in biological processes related to cellular adhesion, junction integrity, and tissue barrier maintenance. The top enriched biological processes included cell–cell junction organization, cell–cell junction assembly, cellular tight junction assembly, cell junction assembly, cell adhesion, cell–cell adhesion, calcium-independent cell–cell adhesion via plasma membrane cell-adhesion molecules, maintenance of the blood–brain barrier, and endothelial cell development (Fig 5B). Molecular function analysis demonstrated a predominance of proteins involved in intermolecular interactions and structural regulation, with significant enrichment of β-catenin binding, protein binding, cell adhesion molecule binding, structural molecule activity, cadherin

binding, virus receptor activity, NF-κB binding, histone decrotonylase activity, E-box binding, and identical protein binding (Fig 5C). Cellular compartment analysis demonstrated predominance of the cell junction, tight junction, catenin complex, adhesion protein etc (Fig 5D). KEGG pathway analysis further highlighted the importance of cell junction and signaling networks, identifying tight junctions, leukocyte transendothelial migration, cell adhesion molecules, adherens junctions, thyroid hormone signaling, and Hippo signaling as major pathways (Fig 5E). Additional enrichment was observed in pathways associated with infectious and disease-related processes, including hepatitis C, pathogenic Escherichia coli infection, epithelial cell signaling in Helicobacter pylori infection, and endometrial cancer. Collectively, these findings suggest that VPA-associated targets are predominantly involved in the regulation of cell adhesion, barrier function, intercellular communication, and signaling pathways that govern tissue homeostasis and disease progression. Enrichment analysis further emphasized pathways and processes tied to Wnt signaling, epithelial cell proliferation, and immune/inflammatory responses, providing a systems-level rationale for how GSK-3β inhibition direct or indirect can coordinate regenerative and anti-inflammatory programs in the damaged intestine.

Survival rates and colon protection following irradiation: Administration of therapeutic VPA at 100 mg/kg b.wt resulted in a higher rate of survival (66%) compared to controls (33%) in the group subjected to WBI 8.5 Gy for 30 days. In the group of mice subjected to 15 Gy abdominal irradiation, VPA administration led to restoration of colon length (measured on day 7) compared to irradiated controls (average length: 15Gy+VPA group = 11.53 cm vs. 15Gy control = 9.9 cm; p=0.001). The in vivo protective effects align with computational evidence that VPA can engage GSK-3β and modify its local dynamics; PPI mapping provides plausible downstream pathways (β-catenin stabilization, reduced NF-κB activity) that explain improved survival and mucosal preservation.

Discussion

We applied an integrative in silico strategy such as molecular docking, long-timescale MD simulations, MM/PBSA energetics, principal component analysis, and protein-protein interaction network mapping to define how VPA might modulate GSK-3β activity and thereby influence Wnt/β-catenin-driven intestinal regeneration and inflammation resolution. This multiscale modelling approach bridges from atomic scale binding mode predictions to systems biology implications of pharmacological action of VPA to counter radiation-induced intestinal injuries. Molecular docking placed VPA within the ATP

pocket of GSK-3β with a predicted binding free energy of -4.7 kcal/mol, substantially weaker than the native ligand and know inhibitor (-8.5 and -7.5 kcal/mol). This difference is consistent with VPA's low molecular weight and limited polar surface area versus larger inhibitors that form an extended network of hydrogen bonds, aromatic and hydrophobic contacts. Importantly, VPA was predicted to contact catalytically relevant residues (for example, Val135, Asp133, Lys85), providing a plausible structural basis for partial active-site modulation. The binding energy of VPA (-4.7 kcal/mol) was considered biologically plausible and pharmacologically relevant, as the estimated inhibition constant (Ki ≈ 0.36 mM) falls below the therapeutic serum concentration of VPA in humans (approximately 0.69 mM i.e 100µg/ml), suggesting that target engagement may be achievable under clinically relevant conditions [27].

Further, MD simulations strengthened the molecular docking i.e after equilibration the VPA-GSK-3β complex remained conformationally stable (protein RMSD plateauing within ~0.15-0.25 nm), and RMSF identified reduced flexibility in active-site residues features that indicate persistent, biologically meaningful occupancy despite moderate static docking affinity. Hydrogen-bond analysis showed significant during the simulation period. Radius of gyration and SASA trends confirmed maintenance of a compact complex and burial of interfacial surfaces upon binding. MM/PBSA decomposition attributed favorable contributions mainly to van der Waals and electrostatic terms, partially counterbalanced by polar solvation penalties consistent with a higher ΔG_{bind} for VPA relative to the native ligand and known inhibitor. Radial distribution function analyses revealed structured hydration and localized ion association near charged groups, underscoring the role of solvent and counter-ions in modulating binding thermodynamics. The favorable energy contributions of residues such as Ile66, Val74, Leu136, Tyr138, Arg148, Leu192, and Cys203 indicate that hydrophobic and polar interactions are major determinants of ligand recognition by GSK-3β. Conversely, residues exhibiting positive energy contributions may impose energetic penalties that modulate binding affinity and contribute to the dynamic nature of the protein–ligand complex. Taken together, the energetic and solvation data indicate that VPA achieves a stable, but not high-affinity, interaction that could be sufficient to perturb kinase dynamics or kinetics in a cellular context. Principal component analysis highlighted that VPA binding alters the landscape of collective motions relative to the reference inhibitor, particularly in modes involving the ATP-binding cleft and adjacent regulatory regions. These changes suggest that VPA may exert modulatory effects on catalytic site accessibility or on

conformational transitions important for activity, offering a mechanistic route by which a moderate binder can produce functional inhibition.

STRING/Cytoscape PPI mapping centered on GSK-3β recovered the canonical destruction-complex partners (CTNNB1, AXIN1, and APC) and downstream effectors linking Wnt signaling to proliferation and inflammation [28]. Network topology identified CTNNB1 and AXIN1 as hub nodes, reinforcing their central role in transmitting GSK-3β perturbations into broad transcriptional programs. Published biochemical evidence such as increased Ser9 phosphorylation of GSK-3β following VPA exposure supports functional attenuation of kinase activity that stabilizes β-catenin, promotes its nuclear translocation, and activates TCF/LEF targets driving crypt stem cell proliferation and epithelial restitution. Concurrent suppression of NF-κB signaling and reduction in pro-inflammatory cytokines (TNF-α, IL-6) reported in preclinical studies provide a coherent mechanistic link between Wnt activation and reduced mucosal inflammation [29]. Our network pharmacology analysis reveals that VPA protects intestinal epithelium through a GSK3β-centered mechanism that simultaneously stabilizes the apical junctional complex and promotes epithelial renewal via β-catenin accumulation. The predicted functional interaction network highlights a strong association with proteins involved in tight junction organization, epithelial barrier maintenance, and cell–cell adhesion. Several key tight junction components, including PARD3, TJP2, TJP3, F11R, and MARVELD2, exhibited very high interaction scores, suggesting a central role in the assembly and stabilization of epithelial junctions. Members of the claudin family, including CLDN24, CLDN8, and CLDN16, further indicate involvement in regulating paracellular permeability and maintaining barrier integrity. The interaction with JAM2 and F11R underscores roles in leukocyte transmigration and endothelial cell communication. Additionally, association with CTNND1 links the network to cadherin-mediated adhesion, cytoskeletal regulation, and signal transduction. Collectively, these findings suggest that the protein is functionally connected to pathways governing tight junction assembly, epithelial polarization, cell adhesion, endothelial barrier function, and tissue homeostasis. This topology supports a dual protective mechanism: VPA's inhibition of GSK3β prevents phosphorylation-dependent degradation of β-catenin, enabling nuclear translocation and transcription of proliferative genes, while concurrently preserving E-cadherin, occludin, and claudin-1 at cell–cell junctions, thereby maintaining paracellular barrier integrity. Functional enrichment highlighted "Wnt signaling pathway," "Adherens junction," "Tight junction," and "HIF-1 signaling pathway" (FDR < 0.05), confirming that VPA's targets converge on these biologically coherent modules. While

STRING/STITCH provides functional associations rather than direct binding, the network topology, literature-supported inhibitory edges, and pathway coherence collectively support a mechanistic model wherein VPA acts as a multi-target radioprotector for intestinal epithelium.

Although VPA is less potent than benchmark GSK-3β inhibitors, its favorable ligand efficiency and well-characterized clinical safety profile make it an attractive repurposing candidate or a minimal scaffold for optimization. Chemical elaboration of VPA-derived cores could improve contact density and affinity while aiming to preserve pharmacokinetics and tolerability; alternatively, combinatorial approaches pairing low-affinity modulation with complementary agents could achieve therapeutic efficacy with reduced off-target risk. Computational methods provide mechanistic hypotheses but cannot replace experimental validation. Key limitations include force-field approximations, finite sampling, approximations inherent to MM/PBSA, and the absence of cellular context (post-translational modifications, protein-protein complexes, and metabolic conversion). We therefore recommend a staged experimental validation plan: in vitro biochemical kinase assays to quantify VPA inhibition and kinetics; cellular assays for Ser9 phosphorylation, β-catenin stabilization and TCF/LEF reporter activity; intestinal organoid models to measure crypt proliferation, differentiation, and barrier function after irradiation; and focused in vivo radioprotection studies assessing dose-response, toxicity, and inflammatory readouts. Transcriptomic and proteomic profiling in these models would further define downstream effectors and candidate biomarkers for monitoring therapeutic response.

The results from our integrative computational analysis suggest that VPA binds to the ATP binding site of GSK-3β protein at a moderate affinity level; stabilizes the local architecture of the protein; and reduces the protein's kinase activity, thus promoting β-catenin mediated pathways and suppressing inflammatory responses. Our in vivo animal studies demonstrate VPA as a potential agent with radioprotective properties and protective effects on colon following radiation exposure. With this computational mechanism-based approach, and in the light of animal studies done as a part of initial findings, it may be concluded that conducting more investigations in animals for demonstrating the role of VPA as a radiomitigator and repositioning VPA as a drug candidate to be used as a GSK-3β inhibitor specifically targeted at gut would be worth consideration as a radioprotector in the context of treating the harmful effects of radiotherapy in the pelvic region.

Acknowledgment

The authors would like to thank Dr. S. Santosh Kumar, Radiation Biology & Health Sciences Division, Bhabha Atomic Research Centre, for his valuable constructive suggestions and critical review of the article. The author also acknowledge the BARC supercomputer facility for allowing to carry MD simulation. The authors would like to acknowledge the technical help provided by Mr. Deepak V. Kathole and Mr. B. A. Naidu. We thank OpenAI's ChatGPT for assistance in improving the clarity and grammar of the manuscript.

Declaration of Conflicting Interests

The author declared no potential conflicts of interest with respect to the research, authorship, and/or publication of this article.

Authors' contributions

Prashasti Sharma performed all in vivo studies, assisted in computational study and drafted manuscript. Whereas Dharmendra Kumar Maurya, help in silico and in vivo studies.

Funding: This work is funded by Department of Atomic Energy, Government of India

References

[1] S. Churnratanakul, B. Wirzba, T. Lam, K. Walker, R. Fedorak, A.B. Thomson, Radiation and the small intestine. Future perspectives for preventive therapy, Dig Dis 8(1) (1990) 45-60.
[2] G. Chen, Y. Han, H. Zhang, W. Tu, S. Zhang, Radiotherapy-Induced Digestive Injury: Diagnosis, Treatment and Mechanisms, Front Oncol 11 (2021) 757973.
[3] T. Luvhengo, U. Khan, T.K. Marumo, Paneth Cells and Lgr5+ Intestinal Stem Cells in Radiation Enteritis, Applied Sciences, 2023, p. 2758.
[4] J. Perochon, L.R. Carroll, J.B. Cordero, Wnt Signalling in Intestinal Stem Cells: Lessons from Mice and Flies, Genes (Basel) 9(3) (2018).
[5] R.J. Walter, S.J. Sonnentag, L. Munoz-Sagredo, M. Merkel, L. Richert, F. Bunert, Y.M. Heneka, T. Loustau, M. Hodder, R.A. Ridgway, O.J. Sansom, Y. Mely, U. Rothbauer, M. Schmitt, V. Orian-Rousseau, Wnt signaling is boosted during intestinal regeneration by a CD44-positive feedback loop, Cell Death & Disease 13(2) (2022) 168.
[6] D. Wu, W. Pan, GSK3: a multifaceted kinase in Wnt signaling, Trends Biochem Sci 35(3) (2010) 161-8.

[7] M. Yang, X. Li, J. Zhan, R. Pan, Z. Yang, M. Zhou, L. Ma, C. Liu, Glycogen Synthase Kinase 3 Is Essential for Intestinal Cell Niche and Digestive Function, Biology (Basel) 14(11) (2025).
[8] B.W. Doble, J.R. Woodgett, GSK-3: tricks of the trade for a multi-tasking kinase, J Cell Sci 116(Pt 7) (2003) 1175-86.
[9] J. Liu, Q. Xiao, J. Xiao, C. Niu, Y. Li, X. Zhang, Z. Zhou, G. Shu, G. Yin, Wnt/β-catenin signalling: function, biological mechanisms, and therapeutic opportunities, Signal Transduction and Targeted Therapy 7(1) (2022) 3.
[10] M.J. Wang, H.Y. Huang, W.F. Chen, H.F. Chang, J.S. Kuo, Glycogen synthase kinase-3β inactivation inhibits tumor necrosis factor-α production in microglia by modulating nuclear factor κB and MLK3/JNK signaling cascades, J Neuroinflammation 7 (2010) 99.
[11] I. Sahin, A. Eturi, A. De Souza, S. Pamarthy, F. Tavora, F.J. Giles, B.A. Carneiro, Glycogen synthase kinase-3 beta inhibitors as novel cancer treatments and modulators of antitumor immune responses, Cancer Biology & Therapy 20(8) (2019) 1047-1056.
[12] G. Chen, L.D. Huang, Y.M. Jiang, H.K. Manji, The mood-stabilizing agent valproate inhibits the activity of glycogen synthase kinase-3, J Neurochem 72(3) (1999) 1327-30.
[13] M. Göttlicher, S. Minucci, P. Zhu, O.H. Krämer, A. Schimpf, S. Giavara, J.P. Sleeman, F. Lo Coco, C. Nervi, P.G. Pelicci, T. Heinzel, Valproic acid defines a novel class of HDAC inhibitors inducing differentiation of transformed cells, Embo j 20(24) (2001) 6969-78.
[14] Y. Leng, M.-H. Liang, M. Ren, Z. Marinova, P. Leeds, D.-M. Chuang, Synergistic Neuroprotective Effects of Lithium and Valproic Acid or Other Histone Deacetylase Inhibitors in Neurons: Roles of Glycogen Synthase Kinase-3 Inhibition, The Journal of Neuroscience 28(10) (2008) 2576.
[15] Y. Zhou, J. Niu, S. Li, H. Hou, Y. Xu, W. Zhang, Y. Jiang, Radioprotective effects of valproic acid, a histone deacetylase inhibitor, in the rat brain, Biomed Rep 3(1) (2015) 63-69.
[16] D. Thotala, R.M. Karvas, J.A. Engelbach, J.R. Garbow, A.N. Hallahan, T.A. DeWees, A. Laszlo, D.E. Hallahan, Valproic acid enhances the efficacy of radiation therapy by protecting normal hippocampal neurons and sensitizing malignant glioblastoma cells, Oncotarget 6(33) (2015) 35004-22.
[17] E.F. Pettersen, T.D. Goddard, C.C. Huang, G.S. Couch, D.M. Greenblatt, E.C. Meng, T.E. Ferrin, UCSF Chimera--a visualization system for exploratory research and analysis, Journal of computational chemistry 25(13) (2004) 1605-12.
[18] O. Trott, A.J. Olson, AutoDock Vina: improving the speed and accuracy of docking with a new scoring function, efficient optimization, and multithreading, Journal of computational chemistry 31(2) (2010) 455-461.
[19] M.J. Abraham, T. Murtola, R. Schulz, S. Páll, J.C. Smith, B. Hess, E. Lindahl, GROMACS: High performance molecular simulations through multi-level parallelism from laptops to supercomputers, SoftwareX 1-2 (2015) 19-25.
[20] M. Bugnon, M. Goullieux, U.F. Röhrig, M.A.S. Perez, A. Daina, O. Michielin, V. Zoete, SwissParam 2023: A Modern Web-Based Tool for Efficient

Small Molecule Parametrization, Journal of Chemical Information and Modeling 63(21) (2023) 6469-6475.
[21] R. Kumari, R. Kumar, A. Lynn, g_mmpbsa—A GROMACS Tool for High-Throughput MM-PBSA Calculations, Journal of Chemical Information and Modeling 54(7) (2014) 1951-1962.
[22] J. Sun, J. Piao, N. Li, Y. Yang, K.Y. Kim, Z. Lin, Valproic acid targets HDAC1/2 and HDAC1/PTEN/Akt signalling to inhibit cell proliferation via the induction of autophagy in gastric cancer, Febs j 287(10) (2020) 2118-2133.
[23] H. Luo, S. Hu, H. Bian, S. Zheng, B. Xiong, Z. Huang, Z. Liu, C. Sun, L. Ma, H. Li, W. Yu, M. Du, H. Chen, W. Lai, [Protective effects of valproic acid on gut barrier function after major burn injury and its mechanism], Zhonghua Wei Zhong Bing Ji Jiu Yi Xue 29(3) (2017) 221-227.
[24] H.-M. Luo, M.-H. Du, Z.-L. Lin, L. Zhang, L. Ma, H. Wang, W. Yu, Y. Lv, J.-Y. Lu, Y.-L. Pi, S. Hu, Z.-Y. Sheng, Valproic Acid Treatment Inhibits Hypoxia-Inducible Factor 1α Accumulation and Protects against Burn-Induced Gut Barrier Dysfunction in a Rodent Model, PLOS ONE 8(10) (2013) e77523.
[25] N.T. Doncheva, J.H. Morris, J. Gorodkin, L.J. Jensen, Cytoscape StringApp: Network Analysis and Visualization of Proteomics Data, Journal of proteome research 18(2) (2019) 623-632.
[26] D. Szklarczyk, R. Kirsch, M. Koutrouli, K. Nastou, F. Mehryary, R. Hachilif, A.L. Gable, T. Fang, N.T. Doncheva, S. Pyysalo, P. Bork, L.J. Jensen, C. von Mering, The STRING database in 2023: protein-protein association networks and functional enrichment analyses for any sequenced genome of interest, Nucleic Acids Res 51(D1) (2023) D638-d646.
[27] M.R. Young, E.K. Bisaccia, L. Romantseva, S.W. Hovey, Valproic Acid Serum Concentration and Incidence of Toxicity in Pediatric Patients, J Child Neurol 37(6) (2022) 461-470.
[28] R. Silva, S.K. Marie, M. Uno, H. Matushita, A. Wakamatsu, S. Rosemberg, S.M. Oba-Shinjo, CTNNB1, AXIN1 and APC expression analysis of different medulloblastoma variants, Clinics (Sao Paulo) 68(2) (2013) 167-72.
[29] B. Ma, M.O. Hottiger, Crosstalk between Wnt/β-Catenin and NF-κB Signaling Pathway during Inflammation, Front Immunol 7 (2016) 378.

Figure and Table Legends

Figure 1: 2D and 3D interaction profiles of GSK-3β complexed with valproic acid and standard inhibitors. Binding orientations are illustrated in the active site of GSK3β, displaying hydrogen bonds, hydrophobic contacts, and key residues involved in ligand stabilization. Two-dimensional interaction maps highlight variations in residue engagement between valproic acid and known inhibitors.

Figure 2: Structural stability and compactness analysis of GSK-3β-ligand complexes during molecular dynamics simulation. A) Root mean square deviation (RMSD), B) Root mean square fluctuation (RMSF), C) Radius of gyration (Rg) represent backbone and residue-level fluctuations in VPA, native ligand and known inhibitor complexes over the simulation trajectory, indicating conformational stability, flexibility, and compactness and D) Radial distribution function (RDF) plots describe atomic interaction density and spatial organization between ligand and protein key residues.

Figure 3: Hydrogen bond analysis and solvent accessibility of GSK-3β–ligand complexes. A) H-bond count are plotted over time to assess structural folding behavior and ligand-binding stability within the protein microenvironment, and B) Solvent-accessible surface area (SASA).

Figure 4: Principal component analysis (PCA) of GSK-3β-ligand systems. PCA highlights dominant collective motions, illustrating conformational space and dynamic clustering patterns of each complex.

Figure 5: Individual amino acid total contributional energy in in interaction of GSK3-β with it native ligand, known inhibitor and VPA.

Figure 6: Protein–protein interaction network analysis. A) Combined network analysis of VPA and GSK-3β and know possible target protein related to intestinal regeneration involved in the WNT/β-catenin signaling pathway. Functional enrichment analyses of the VPA-associated seed proteins for B) Biological process, C) Molecular function, D) Cellular component, and E) KEGG pathway enrichment.

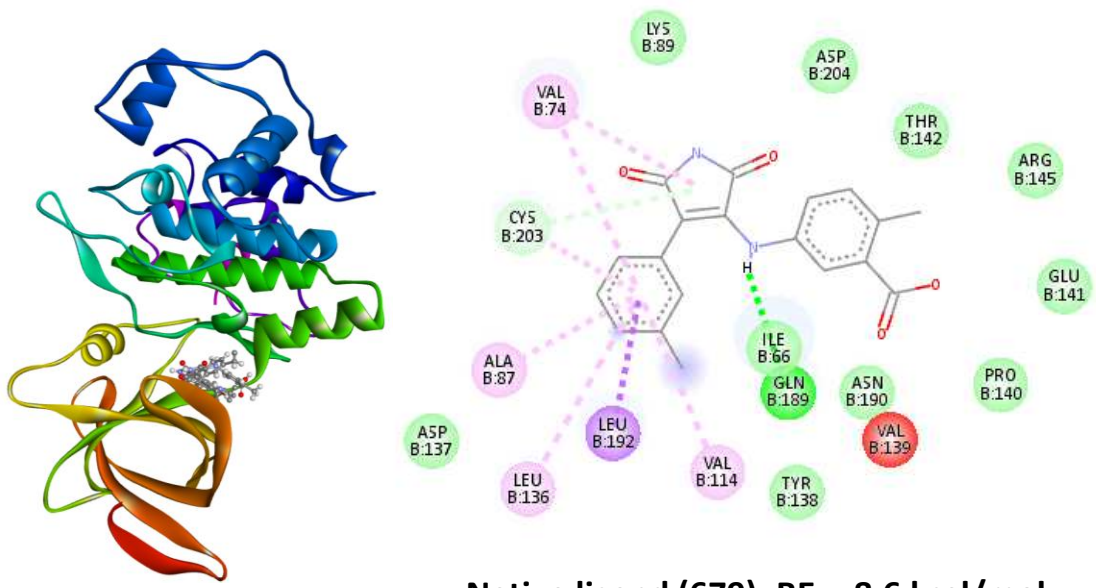
Figure 7. In vivo radioprotection by VPA. A) Mice survival, B) Mice weight, C) Colon restoration and D) Colon length

Figure 8: Schematic diagram illustrating the proposed molecular mechanism by which VPA might mediates regeneration in intestinal epithelium. VPA is hypothesized to interact directly with GSK-3β, resulting in downstream

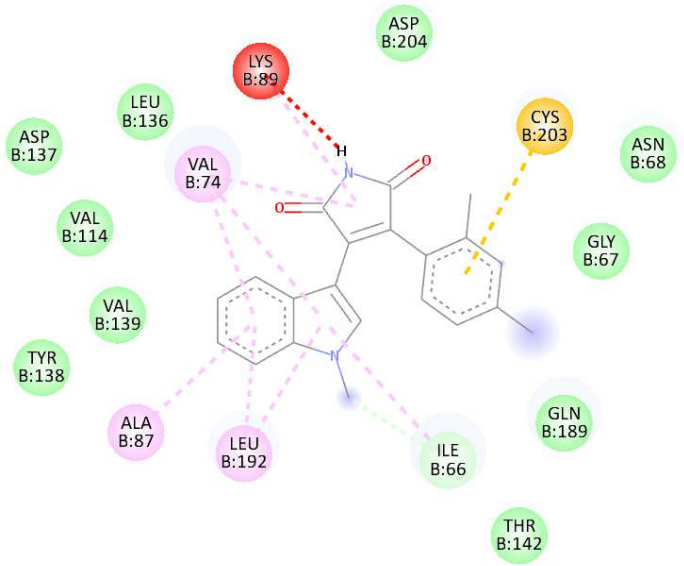
modulation of WNT/β-catenin signaling pathways. Inhibition of GSK3-β activity may promote β-catenin stabilization, enhance epithelial stem cell proliferation, and facilitate tissue repair. The integrated modulation of these signaling axes potentially attenuates inflammation, supports mucosal regeneration, and contributes to improved recovery following intestinal injury

Table 1: Binding free energy estimation of GSK-3β-ligand systems. Molecular mechanics Poisson-Boltzmann surface area (MM/PBSA) results present comparative binding free energies of VPA, native ligand and known inhibitor.

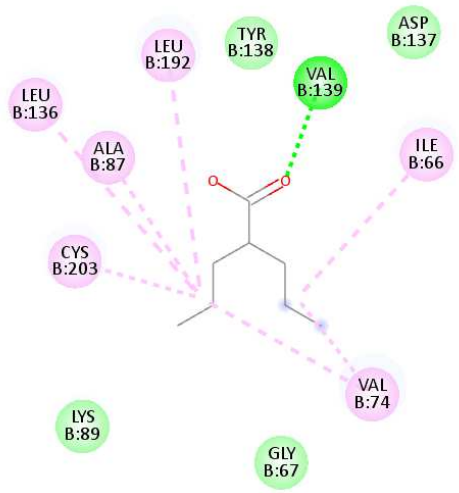
Fig. 1: 2D and 3D Interaction of between GSK3-beta with it native inhibitor, known inhibitor and VPA



Native ligand (679), BE= -8.6 kcal/mol

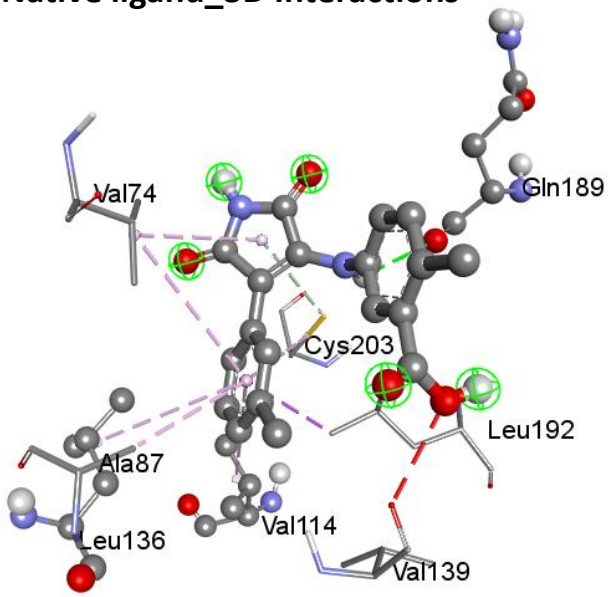


Known Inhibitor (SB216763), BE= -7.6 kcal/mol

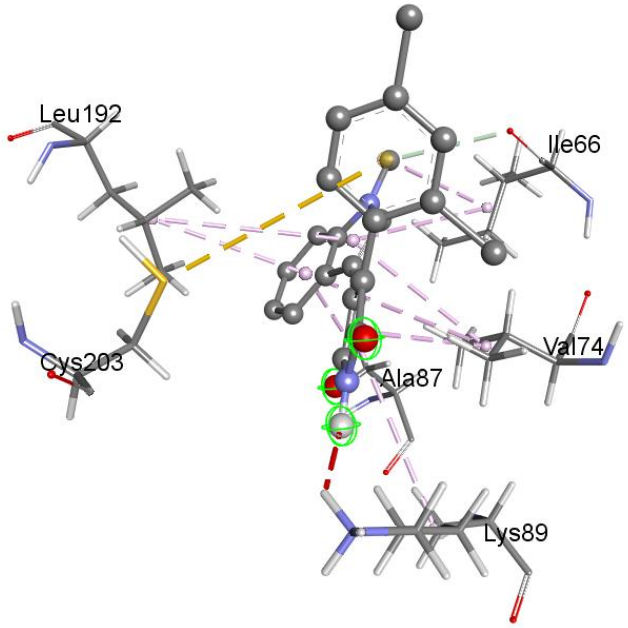


VPA, BE= -4.7 kcal/mol

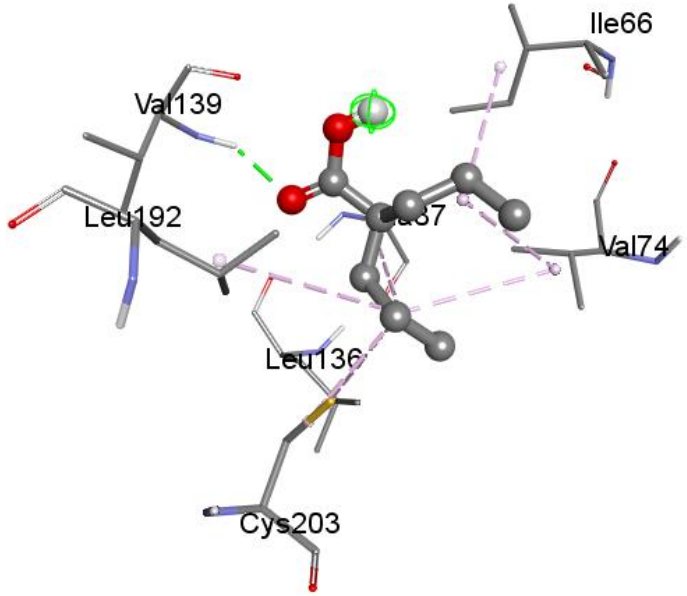
Native ligand_3D Interactions



SB216763 _3D Interactions



VA_3D Interactions

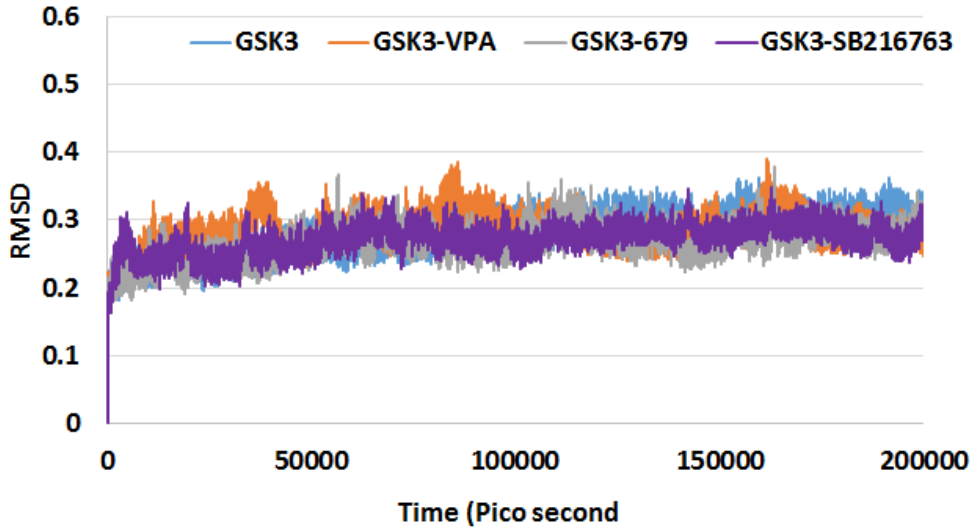


Common interactive residues

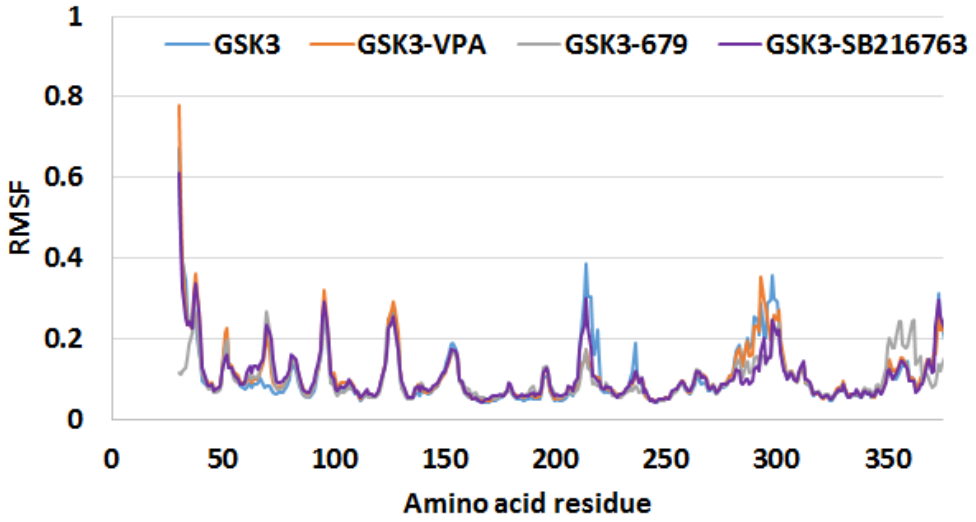
VAL74
LYS89
CYS203
ALA87
LEU136
LEU196
TYR138
VAL139
ASP137
ILE66

Fig. 2: MD simulation of GSK3-beta with it native inhibitor, known inhibitor and VPA

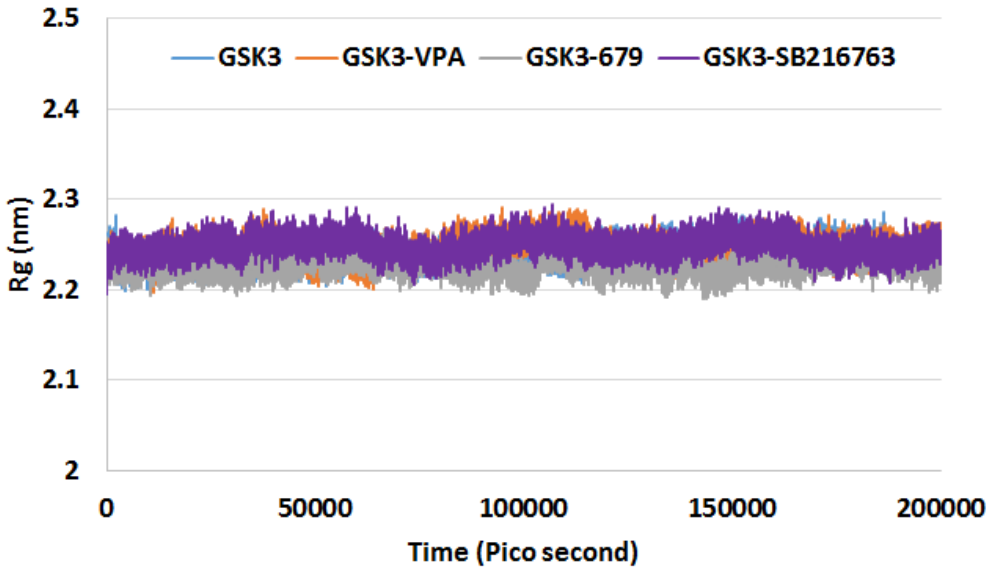
A)



B)



C)



D)

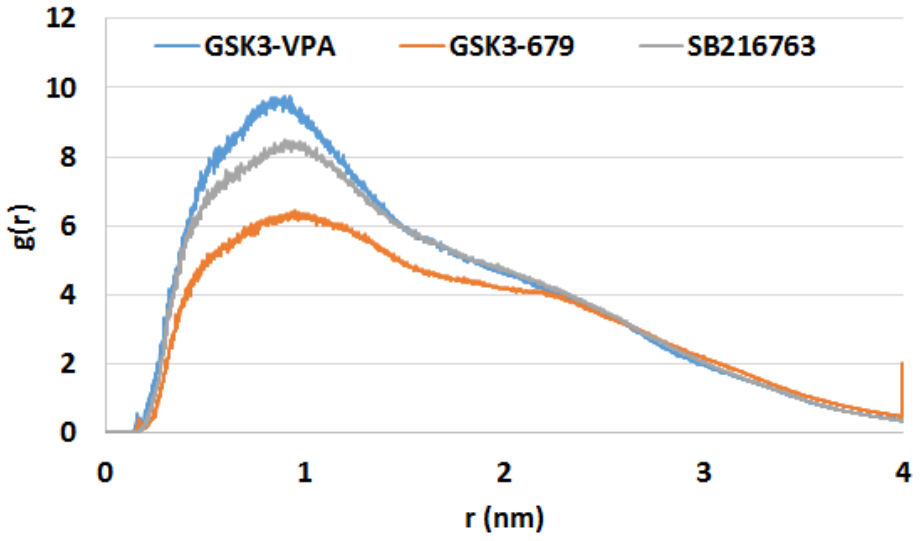


Fig. 3: H-bond and SASA analysis between GSK3-beta with it native inhibitor, known inhibitor and VPA throughout simulation

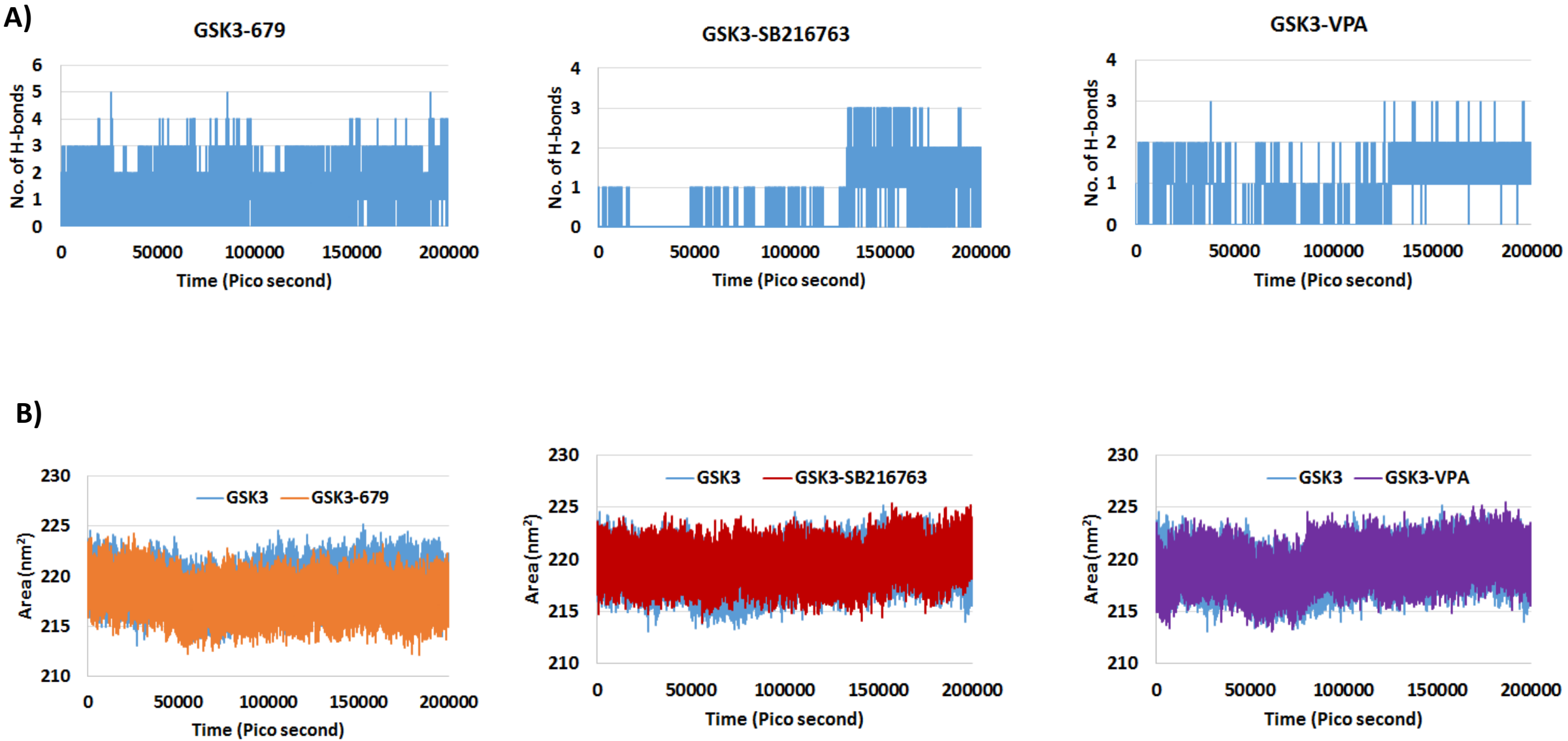


Fig. 4: PCA analysis of GSK3-beta with it native inhibitor, known inhibitor and VPA throughout simulation

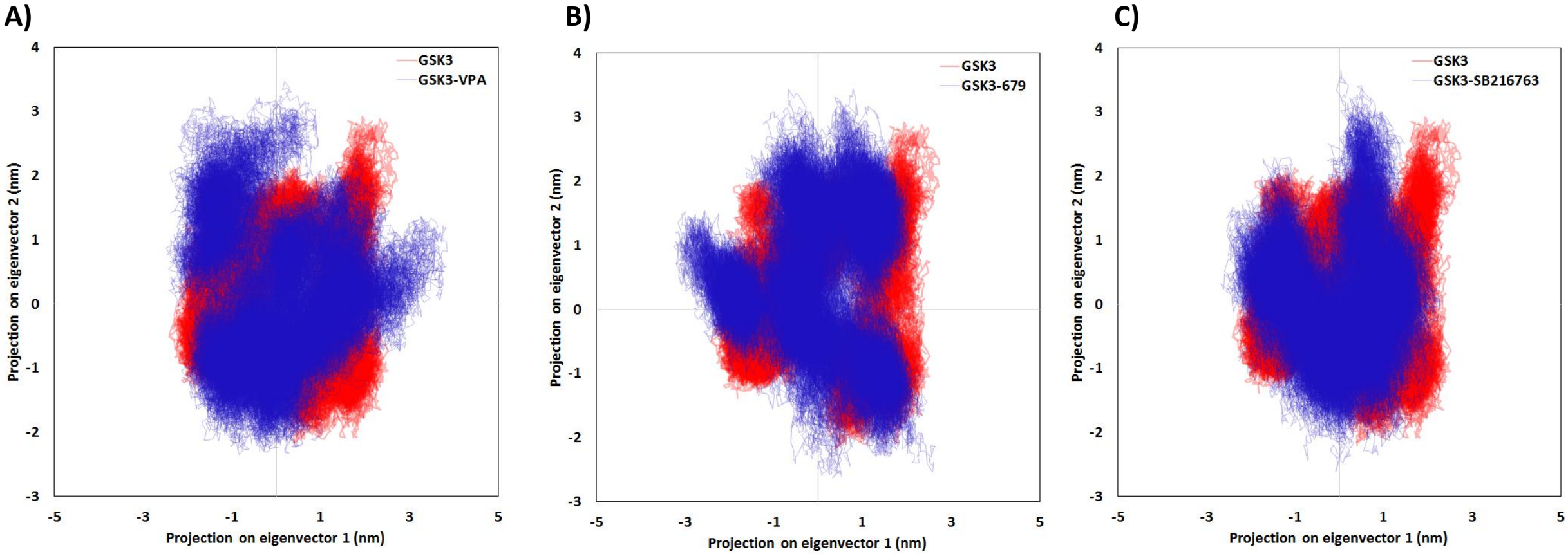


Fig. 5: Individual amino acid total contributional energy in in interaction of GSK3-beta with it native inhibitor, known inhibitor and VPA

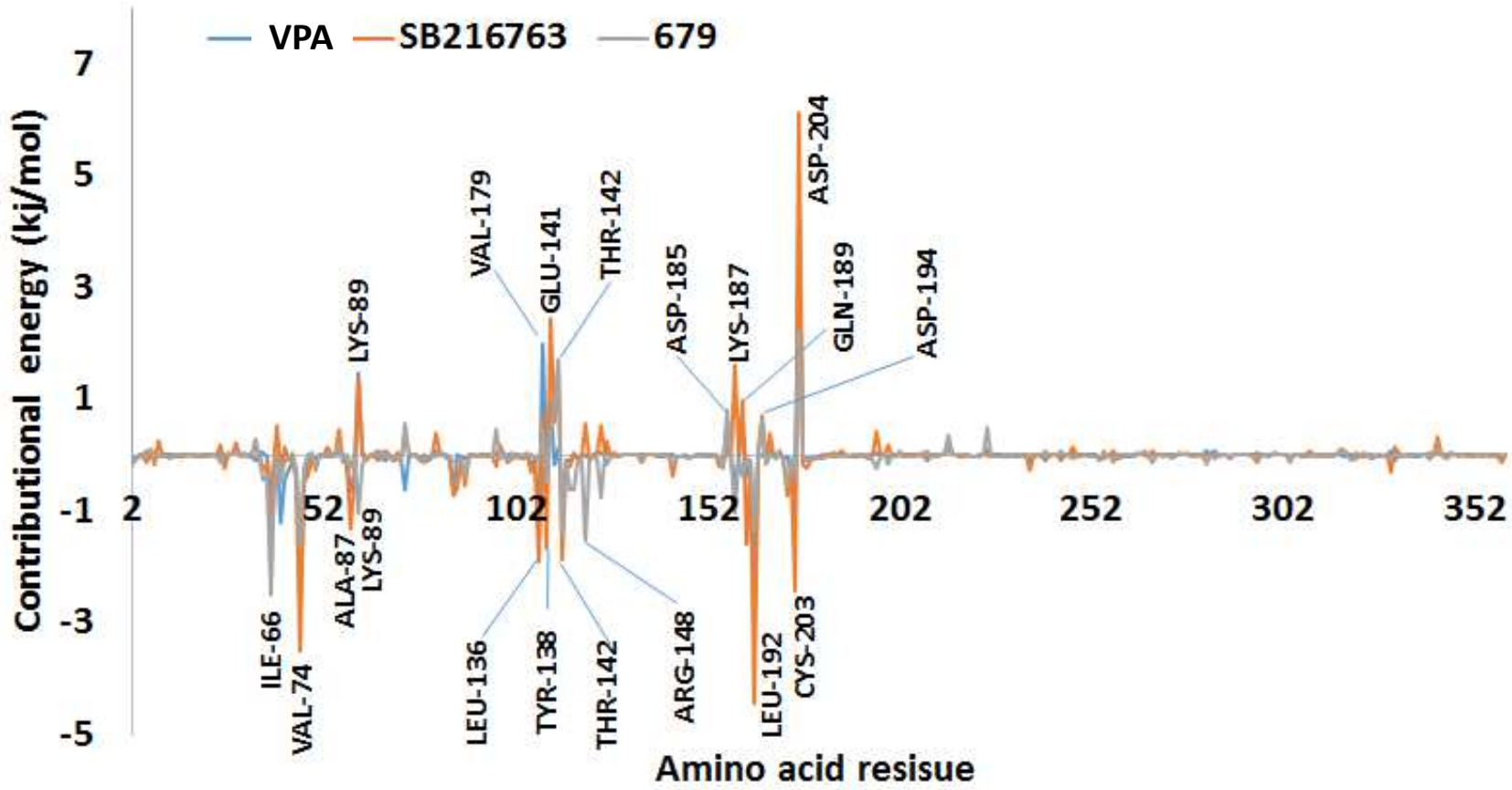
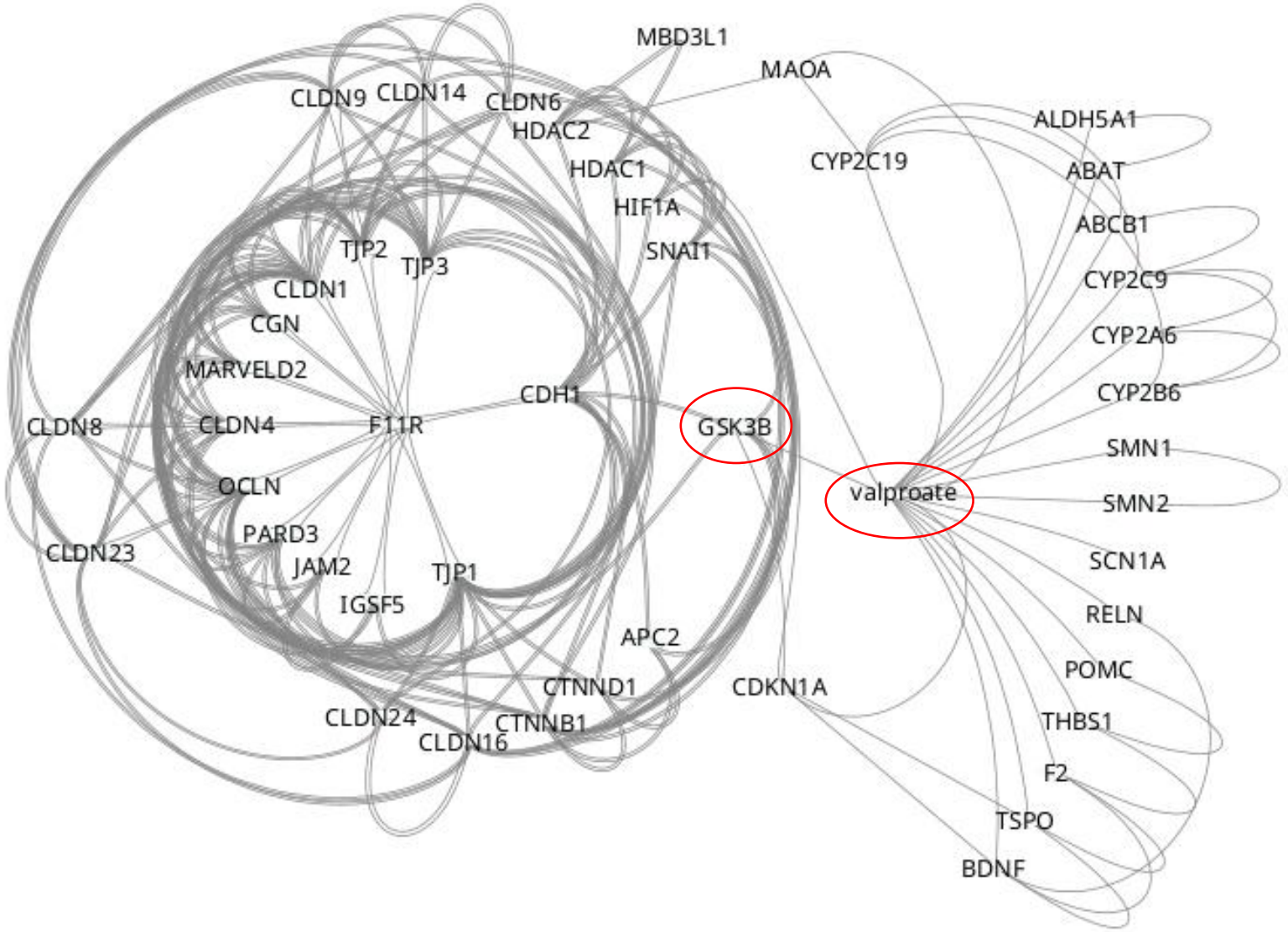


Fig. 6: STRING/STRITCH-based PPI analysis between players centered with GSK-3β and VPA

A



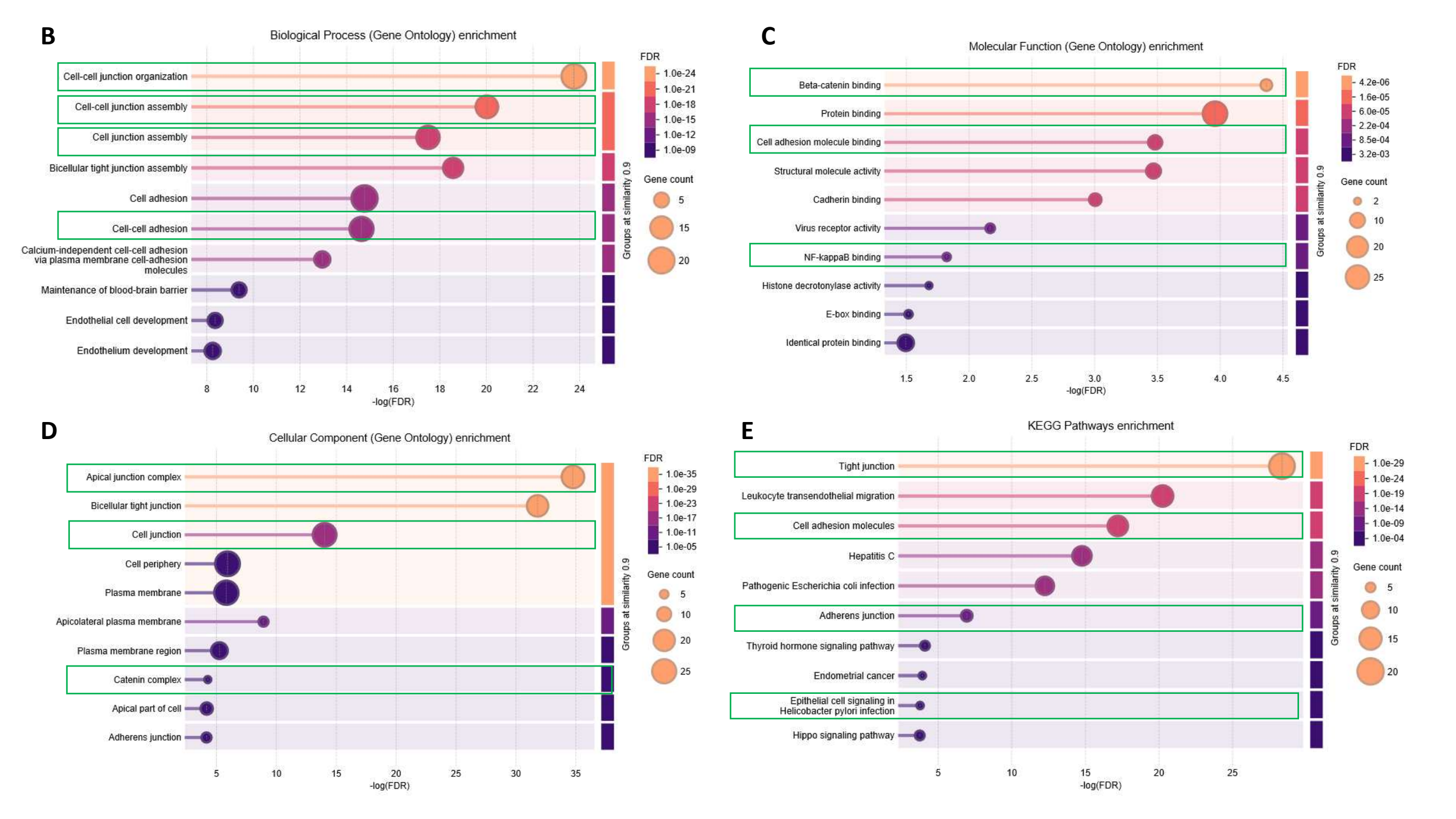
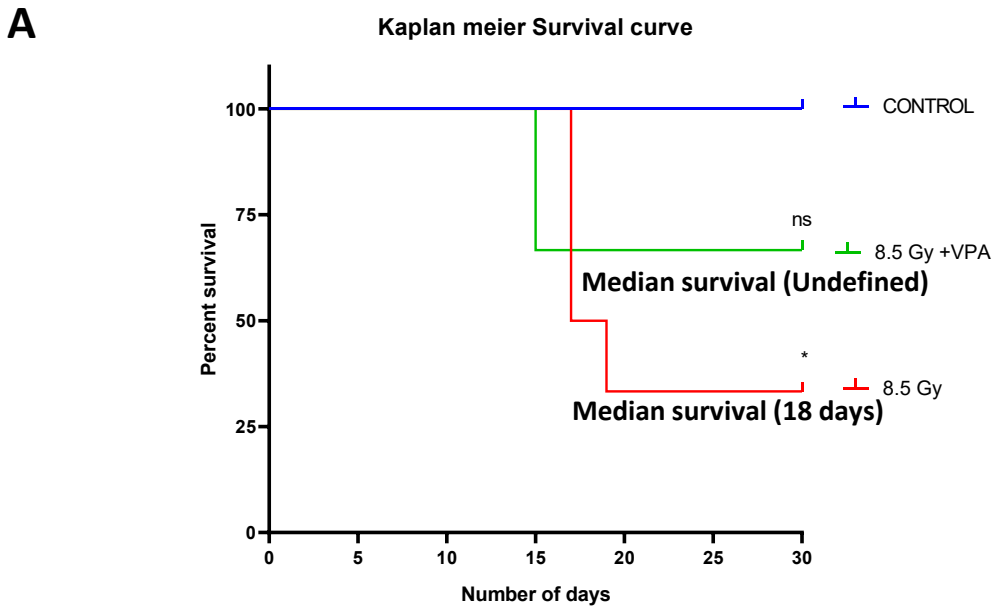
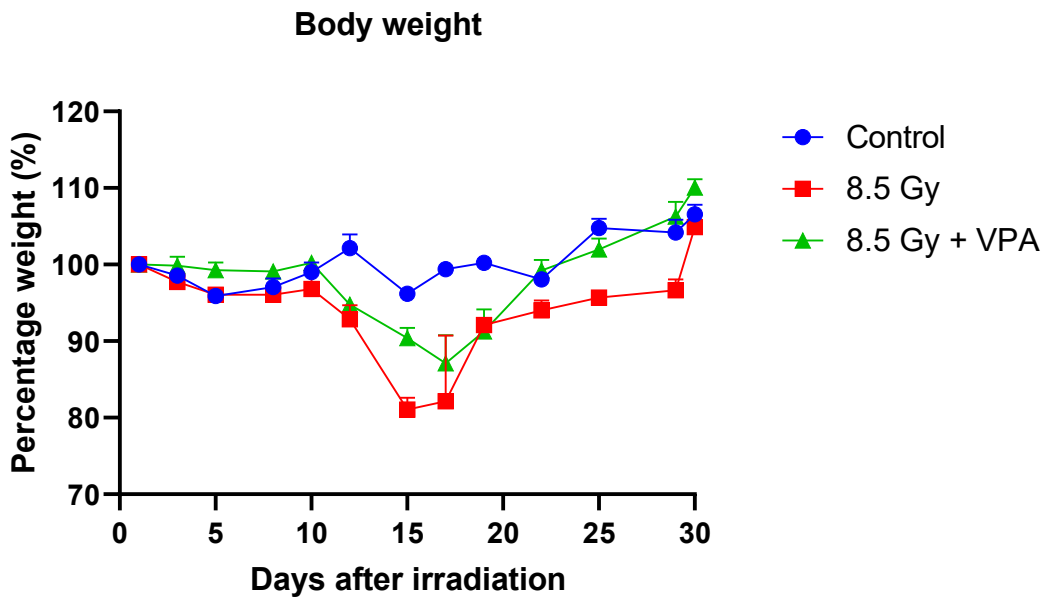
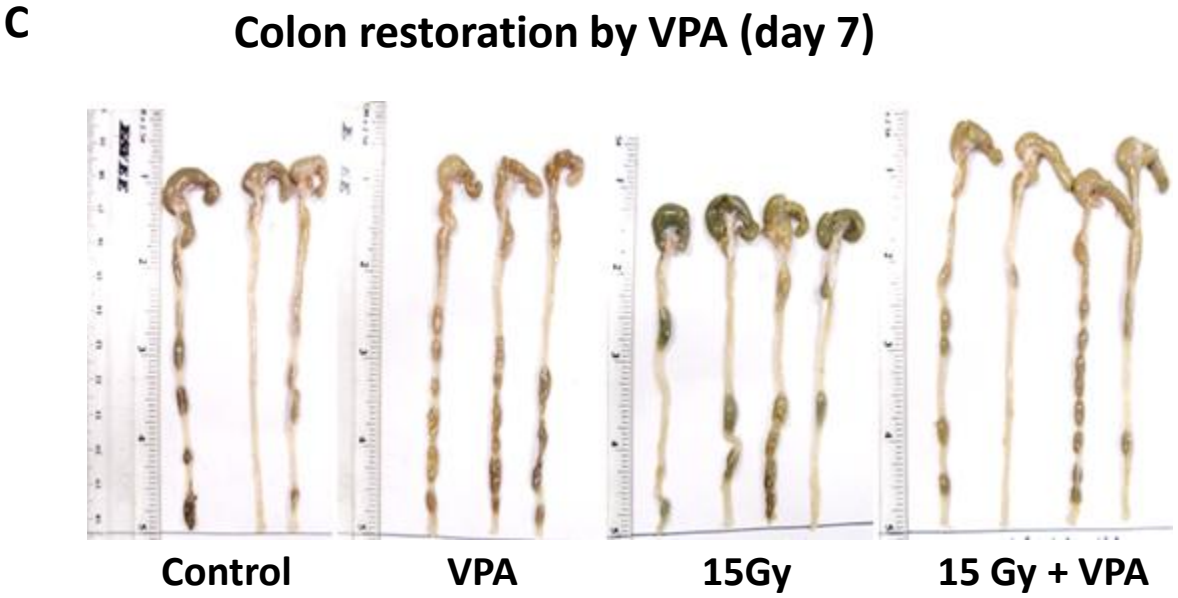

B
Biological Process (Gene Ontology) enrichment
Cell-cell junction organization
Cell-cell junction assembly
Cell junction assembly
Bicellular tight junction assembly
Cell adhesion
Cell-cell adhesion
Calcium-independent cell-cell adhesion via plasma membrane cell-adhesion molecules
Maintenance of blood-brain barrier
Endothelial cell development
Endothelium development
8 10 12 14 16 18 20 22 24
-log(FDR)
Groups at similarity 0.9
FDR
1.0e-24
1.0e-21
1.0e-18
1.0e-15
1.0e-12
1.0e-09
Gene count
5
15
20
C
Molecular Function (Gene Ontology) enrichment
Beta-catenin binding
Protein binding
Cell adhesion molecule binding
Structural molecule activity
Cadherin binding
Virus receptor activity
NF-kappaB binding
Histone decrotonylase activity
E-box binding
Identical protein binding
1.5 2.0 2.5 3.0 3.5 4.0 4.5
-log(FDR)
Groups at similarity 0.9
FDR
4.2e-06
1.6e-05
6.0e-05
2.2e-04
8.5e-04
3.2e-03
Gene count
2
10
20
25
D
Cellular Component (Gene Ontology) enrichment
Apical junction complex
Bicellular tight junction
Cell junction
Cell periphery
Plasma membrane
Apicolateral plasma membrane
Plasma membrane region
Catenin complex
Apical part of cell
Adherens junction
5 10 15 20 25 30 35
-log(FDR)
Groups at similarity 0.9
FDR
1.0e-35
1.0e-29
1.0e-23
1.0e-17
1.0e-11
1.0e-05
Gene count
5
10
20
25
E
KEGG Pathways enrichment
Tight junction
Leukocyte transendothelial migration
Cell adhesion molecules
Hepatitis C
Pathogenic Escherichia coli infection
Adherens junction
Thyroid hormone signaling pathway
Endometrial cancer
Epithelial cell signaling in Helicobacter pylori infection
Hippo signaling pathway
5 10 15 20 25
-log(FDR)
Groups at similarity 0.9
FDR
1.0e-29
1.0e-24
1.0e-19
1.0e-14
1.0e-09
1.0e-04
Gene count
5
10
15
20

Fig. 7: In vivo radioprotection by VPA. A) Mice survival, B) Mice weight, C) Colon restoration and D) Colon length







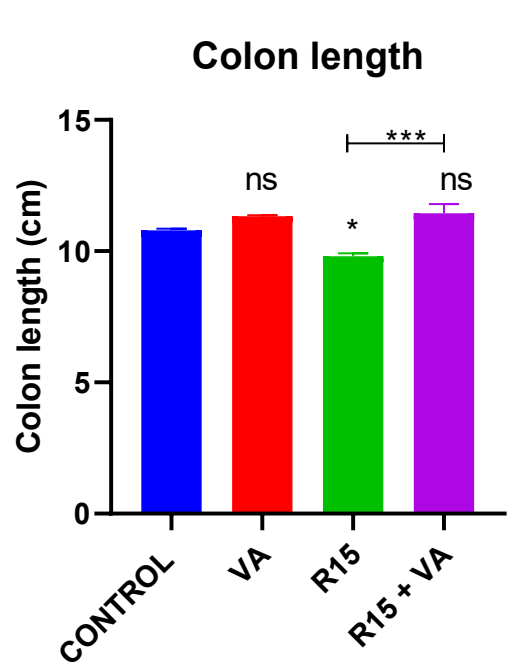
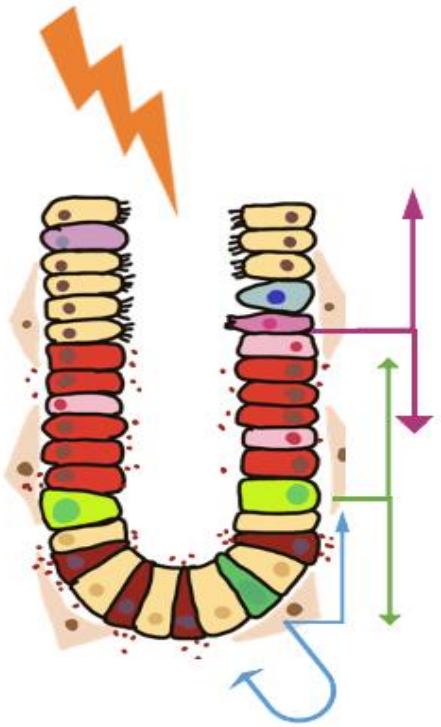
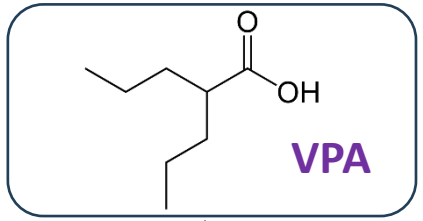


Fig 8. Proposed molecular mechanism of VPA mediated intestinal regeneration

Radiation Induced Intestinal Injury



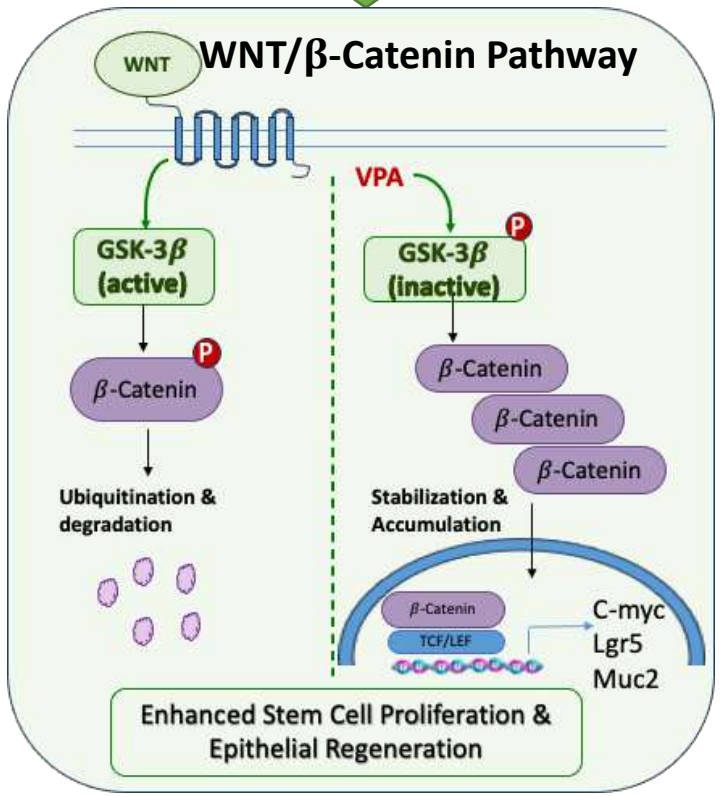
- Epithelial Damage
- Barrier dysfunction
- Inflammatory Cytokines ↑
- Stem Cell loss/Impaired proliferation
- Imbalanced WNT and Notch signaling



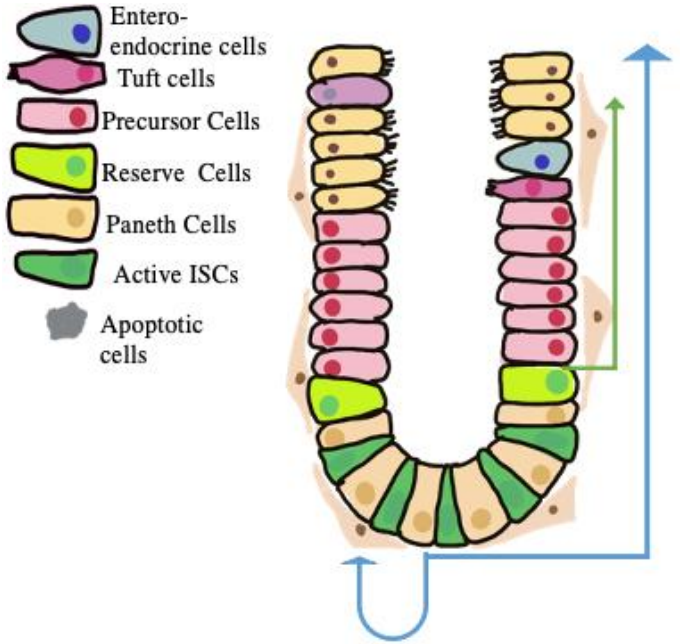
Direct Interaction/Inhibition
(e.g. via binding to allosteric site)

GSK-3 β (P) ↓

Decreased activity



Recovery /Homeostasis (VPA-Treated)



- Intact epithelial barrier
- Tight Junctions ↑
  (ZO-1, Occludin,Claudin-1)
- Inflammation ↓
- Lgr5+ stem cell expansion ↑
- Mucosal regeneration
- Restored cell lineage balance

Supplementary Files

This is a list of supplementary files associated with this preprint. Click to download.

- Table1MMPBSAfreeenergy.docx
- Graphicalabstract.pptx